

# Generation and application of bright coherent extreme ultraviolet radiation

Lap Van Dao\*<sup>1,2</sup>, Khuong Ba Dinh<sup>1,3</sup>, Khoa Anh Tran<sup>1</sup>, Peter Hannaford<sup>1</sup>  
Centre for Quantum and Optical Science,

<sup>1</sup>Swinburne University of Technology, Melbourne 3122, Australia; <sup>2</sup>Graduate University of Science and Technology, Vietnam Academy of Science and Technology, Hanoi, Vietnam; <sup>3</sup>University of Science and Technology, University of Danang, Vietnam;

## ABSTRACT

We study the use of a second driving beam to enhance the phase matching and also to create wave mixing and parametric amplification in extreme ultraviolet region. New methods for studying coherent processes in atoms and molecules and for imaging with high spatial resolution have been proposed and developed

**Keywords:** High order harmonic generation, Extreme ultraviolet radiation, Coherent diffraction imaging, ultrafast laser

## 1. INTRODUCTION

When atoms or molecules interact with an intense laser field, high-order harmonics of the incident radiation may be generated. This process provides methods to produce short pulses of coherent radiation in the extreme ultraviolet (XUV) and soft X-ray region. Such source opens up new applications such as in time-resolved studies of atoms and molecules [1], and coherent diffractive imaging [2] in the XUV and soft X-ray range. A large number of studies has been carried out in order to understand the physics of the high order harmonic generation (HHG) process and to enhance the harmonic intensity and photon energy. Coherent radiation in the water window (below the carbon K edge at 4.4 nm), was reported by using femtosecond lasers pulse as driving pulse [3]. In parallel with the extension of harmonic orders, many experiments have investigated the spatial and temporal characteristics of the harmonic emission, revealing the unique properties of this XUV source: good coherence, ultrashort (attosecond) pulse duration, high brightness, high repetition rate, tunability, compactness, etc.

From the point of view of fundamental research, high-order harmonic generation is an example of nonlinear physics, where simple pictures can be used to describe strongly non-perturbative processes with the time-dependent Schrodinger equation. This highly nonlinear process leading to the up-conversion of low energy photons into XUV or X-ray photons can be conceptually understood classically in the so-called three-step model [4] where an electron is first liberated from an atom through strong field ionization, then is accelerated by the laser field, and finally is recombined with the parent ion, emitting any excess energy as a high-energy photon. In the three-step model the generation of high-order harmonics has been a single-emitter picture (atom or molecule). Under real experimental conditions, it is in fact the coherent superposition of the radiation from a very large number of emitters (atoms or molecules) that is responsible for the HHG output. The nature of this superposition is a relatively complex problem known as ‘phase-matching’ that depends on the spatial and temporal variation of the emitter density and propagation of the laser field within the interaction volume [5]. The phase matching between the fundamental laser field and the harmonic field plays a very important role in HHG, especially for the generation of high flux radiation. Although the harmonic generation efficiency has been significantly enhanced in recent years research to achieve harmonics with low beam divergence as well as good spatial beam quality is important to attain bright harmonic x-ray sources. Efficient harmonic generation requires good phase matching between the generated harmonics and the driving laser pulse and efficient coupling of an intense laser pulse with a large number of atoms.

The wave-packet created by the laser field plays a fundamental role in understanding the quantum picture and provides a bridge between the quantum picture and the classical concept of the trajectory of a particle. The motion of the wave-packet reflects the time evolution of a coherent superposition of the system. Useful information regarding the discrimination and visualization of the wave-packet dynamics can be obtained from time-resolved photoelectron imaging

because of the sensitivity of the photoelectron angular distribution to the electronic symmetry. The HHG process involves a coherent recombination of wave-packets and can be used to study wave-packet properties [1]. In a HHG experiment the propagation and phase of the fundamental and harmonic fields depend on the optical properties of the medium and are reflected in the observed harmonic intensity through the so-called phase mismatch factor. A perturbation of the propagation or moving of free electrons process can lead to a change in the harmonic phase and therefore to modification of the total output of harmonic radiation.

Novel imaging and labelling techniques in visible optical microscopy, where a resolution of down to 20 nm can be achieved in special cases, can be used to study dynamic processes in living cells and nanostructures. To obtain very high resolution illumination at short wavelengths, high resolution lenses are required. In visible light microscopes, lenses can be made from precision-shaped glass, while magnetic fields and zone plates are used for focusing electrons and X-rays, respectively. When focusing optics are applied in imaging, high-frequency information cannot be collected by the lens and is excluded in the reconstruction of the image, which limits the resolution, and lens imperfections cause aberrations in the image. Optics in the X-ray and Extreme Ultraviolet (XUV) regions are more difficult to produce and are less effective. To avoid the use of lenses coherent diffraction imaging (CDI), or “lens-less imaging” [3], has been developed.

In this paper we show that a second driving beam can be used to enhance the phase matching and also to create wave mixing and parametric amplification [6]. The combination of two driving fields with controllable intensity ratio opens a new way for the generation of additional frequency components which is a step towards obtaining attosecond pulses with high intensity in the soft X-ray region. Because the HHG spectrum depends on the structure of the atom or molecule a new method for studying coherent processes in atoms and molecules has been proposed and developed [7]. In addition, the use of a table-top HHG source for coherent diffractive imaging is very promising for spatial resolution of sub-10 nm [8].

## 2. EXPERIMENT

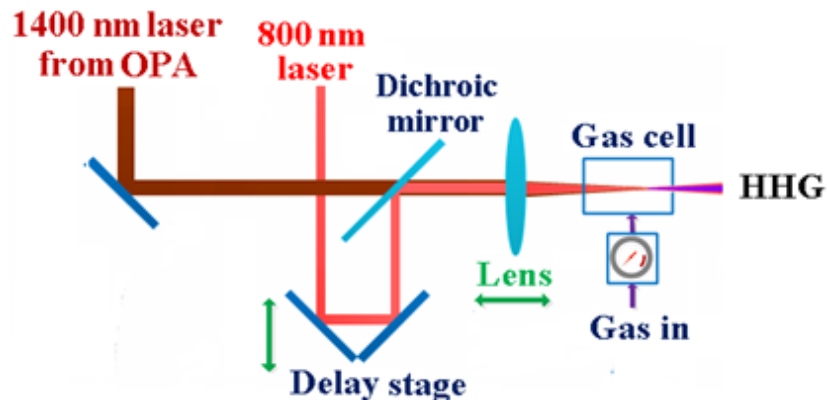


Figure 1. Arrangement of the two colour laser beams

A 800 nm, 10 mJ, 30 fs, 1 kHz repetition rate laser beam is split into two beams, with pulse energies of 6 mJ and 4 mJ. The 6 mJ beam is used to pump a three-stage optical parametric amplifier (OPA) system to generate an infrared (IR) driving pulse at 1400 nm with energy up to 1.6 mJ and duration 40 fs. The 4 mJ (800 nm) pulse or a part (~1 mJ) of this pulse is used as an amplifier or controller field. The 1400 nm and the 800 nm pulse are aligned in the same direction or at a very small angle to each other by a dichroic mirror. The experimental arrangement is shown in Fig. 1. Further details of the HHG setup and detection system are described elsewhere [3,9]. The polarizations of the two pulses can be varied. The focus position of the two beams can be shifted relative to each other which allows control of the intensity and the spatial profile of the output XUV radiation. The time delay between the two pulses is controlled by a motorized delay stage with 0.1 fs resolution. Positive delay time implies that the 800 nm pulse precedes the 1400 nm pulse. The laser beams are used to drill an exit pinhole in a thin aluminium plate allowing straight-forward handling, and no further alignment procedure along the optical axis of the 1400 nm or/and 800 nm pulse is needed. The diameter of the two beams at the focus is ~150 μm. A long (~30 mm) cell filled with argon gas at a pressure up to 350 Torr is used as the interaction medium. The harmonic emission enters a flat-field XUV spectrometer comprising a slit, concave grating, and

a cooled 14-bit CCD camera. A non-collinear configuration of the two beams helps to spatially separate the wave-mixing field from the 1400 nm and 800 nm beams. A collinear configuration of the two beams is applied for precise control of the time evolution of the output.

### 3. CREATION OF EXTREME ULTRAVIOLET RADIATION

#### 3.1 Phase-matched generation

Using a 400 mm focal length lens for focusing the single driving laser pulse (800 nm or 1400 nm), the radius of the focused intensity distribution of the femtosecond laser beam can be varied from approximately 45  $\mu\text{m}$  to 100  $\mu\text{m}$  over which the Rayleigh range varies from 5 to 20 mm. Taking into account defocusing due to the generated plasma, the effective focused intensity is about  $2.10^{14}$  W/cm<sup>2</sup>. At a fixed pressure and a fixed position of the focus optimization of the harmonic beam is conducted by varying the aperture applied to the driving laser beam. This is mainly due to optimization of the effective f-number, the beam quality of the laser beam, the complex interplay between the intrinsic phase of the harmonic emission and the laser phase and the change of ionization rate. The good beam quality in the harmonic far field and the small bandwidth of the harmonic spectrum indicate that phase matching is mainly satisfied along the propagation axis of the pump pulse [9]. The effective spectral range and the relative weight of single harmonic orders of the harmonic beam can be also controlled by the phase-matching parameters, e.g. the gas pressure and the intensity of the laser pulses. By an appropriate choice of species of gas, gas pressure, interaction length, position of the laser focus and intensity and diameter of the laser beam, the harmonic emission can also be phase-matched and confined to just a few harmonic orders when an 800 nm pulse is used as the driving pulse. A typical HHG spectrum is shown in Fig. 2 when argon gas is used as the active medium for a driving pulse at 800 nm (Fig. 2a) and 1400 nm (Fig. 2b).

When the focus position of the driving pulses is varied from outside (negative) to inside (positive) of the gas cell the interaction length is increasing (Fig. 2a) and the HHG intensity increases quadratically with the interaction length and thus indicates that the harmonic emission is phase-matched for this spectral band width. The maximum HHG intensity is obtained at a focus position  $\sim 1$ mm from the exit pinhole. When the interaction length is long the HHG intensity is decreased because of self-absorption and a large phase-mismatch. When a 1400 nm pulse is used as the driving pulse (see Fig. 2b) the optimized value for the pressure is found to be  $p_{\text{Ar}} = 280$  Torr. For  $p_{\text{Ar}} < 200$  Torr the harmonic intensity increases quadratically with pressure. For  $p_{\text{Ar}} > 300$  Torr the variation of the harmonic emission intensity is dominated by re-absorption which occurs very strongly for harmonics with wavelength  $> 30$  nm.

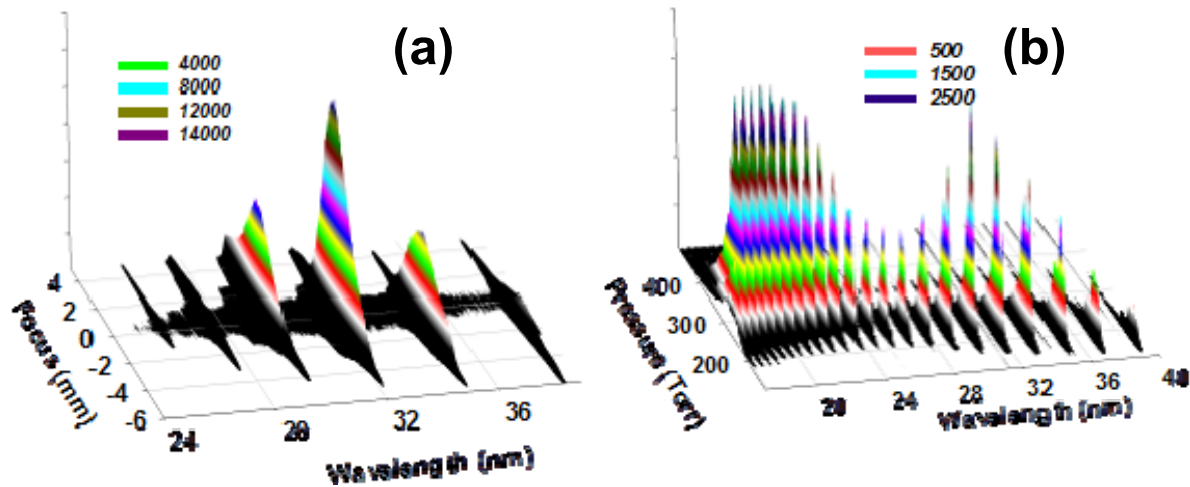


Figure 2: Phase-matched generation of harmonics using a 800 nm and 1400 nm driving pulse for different interaction lengths (a) and gas pressures (b). Well-resolved odd-number harmonics with high spatial coherence are observed in this case.

### 3.2 Parametric amplification

When the intensity of the 800 nm pulse is  $> 7 \cdot 10^{14}$  W/cm<sup>2</sup> around the focus the ionization fraction is very high ( $> 15\%$ ) at the peak of the pump pulse. The spectrum of the HHG radiation generated by the 800 nm driving pulse is complex: not only odd orders but also even orders are generated and the beam profile is broad. The intensity of radiation below 20 nm is very weak because the phase-mismatch is large. The high-order harmonic radiation can be generated at wavelengths down to 16 nm when an 800 nm pulse, a 1400 nm pulse or both pulses are applied. The intensity of the XUV radiation is much higher (by more than an order of magnitude) when a 1400 nm pulse with intensity of  $\sim 1.5 \cdot 10^{14}$  W/cm<sup>2</sup> is applied and the two pulses are overlapped, i.e., for zero time delay (Fig. 3). This indicates that parametric amplification processes can be considered [6]. A minimum in the spectrum can be seen at  $\sim 51$  eV (24 nm) where a Cooper minimum caused by destructive interference of the 5s and 4d transition dipole moments is expected [10]. The observation of a Cooper minimum in the amplified spectrum indicates that a combination of single-atom responses in the nonlinear atomic dipole moment can be used in a theoretical treatment.

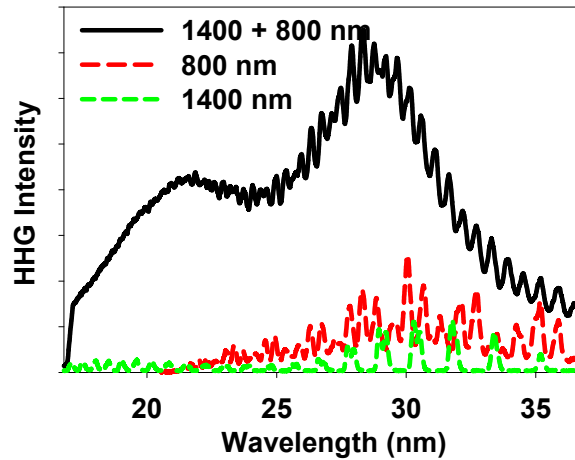


Figure 3. Amplification of extreme ultraviolet radiation with a high intensity 800 nm pulse. The HHG radiation with only one of these pulses such as 800 nm (red long dashed line) and 1400 nm pulses is also shown.

## 4. PERTURBATIVE WAVE-MIXING IN EXTREME ULTRAVIOLET REGION.

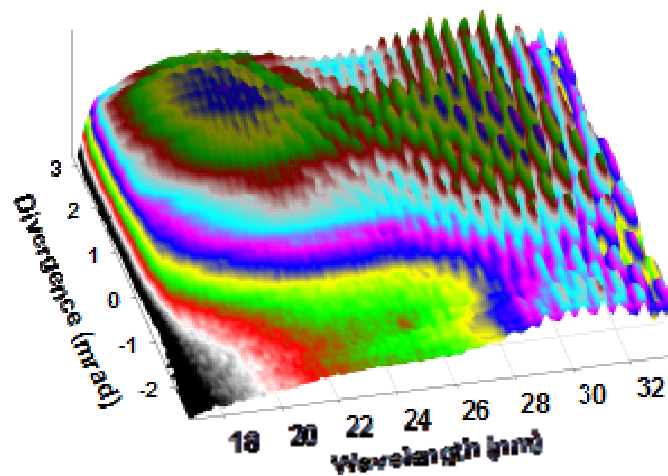


Figure 4: HHG spectrum versus angular divergence at the focus plane of the spectrometer at a delay time of  $\sim 10$  fs between the 1400 nm and 800 nm pulses. The two beams are aligned at angle of  $10^0$ .

When the intensity of the 800 nm pulse is kept low ( $\sim 10^{14}$  W/cm<sup>2</sup>) to avoid strong ionization of the gas medium we are able to observe the wave-mixing in extreme ultraviolet region. In this case the 800 nm beam is aligned at a very small angle ( $< 10^\circ$ ) to the direction of the 1400 nm beam in the vertical plane (Y direction). When the 800 nm pulse is absent or at very long delay times ( $> -200$  fs) we obtain phase-matched radiation along the propagation direction of the 1400 nm driving pulse. The spectrum of the XUV radiation varies markedly with the influence of the second (800 nm) pulse. The addition of a second optical field whose frequency is not commensurate with that of the primary field creates additional frequency components in the HHG spectrum. The spectrum and spatial features, which are observed on the CCD, are modified with the delay time between the two pulses. In Fig. 4 we show the spectrum versus divergence from 1400 nm beam direction axis for a fixed time delay  $\sim 10$  fs, as an example. The discrete spatial and spectral peaks in the CCD image are caused by frequency mixing of the two fields - the harmonic field generated by the 1400 nm driving beam and the delayed 800 nm controlling field. The spectrum exhibits distinguishable peaks which indicate the position of the wave-mixing radiation. The addition of the 800 nm field gives rise to off-axis radiation at different angles in the vertical Y direction of the detector. To emit a single XUV photon conservation of energy and momentum for the generation of the resulting XUV emission need to be considered and parity conservation requires that for a dipole transition the wave function of the continuum electron and the ion together must be in a state of different parity to that of the original ground state [11]. Therefore, only the net absorption of an odd total number of photons  $n = n_1 + n_2$  can lead to photon emission. These selection rules can be written alternatively as:  $\omega_q = n_1\omega_1 + n_2\omega_2$ ;  $k_q = n_1k_1 + n_2k_2$ ;  $n_1 + n_2 = 2j + 1$ , where  $j$  is an integer,  $\omega_1$  is the carrier frequency of the 1400 nm field and  $\omega_2$  is the carrier frequency of the 800 nm field. From this approach, it is possible to produce a radiated frequency  $\omega_q = (2j + 1)\omega_1 \pm n(\omega_2 - \omega_1)$  and along directions  $k_q = (2j + 1)k_1 \pm n(k_2 - k_1)$  for various  $(j, n)$  combinations.

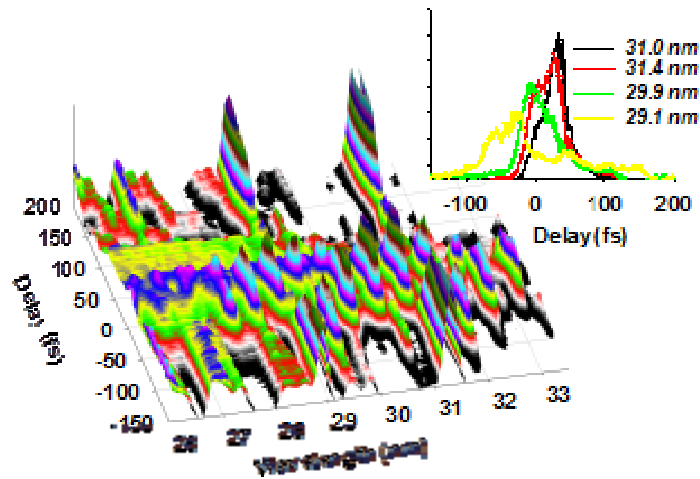


Figure 5: HHG spectrum generated by a 1400 nm driving pulse versus delay time of the 800 nm controlling pulse in a co-propagating configuration. The inset shows the high spectral resolution of the radiation versus delay time of the two beams.

For a detailed study of the time evolution of the mixing process a collinear propagation of the two fields is used. In this configuration the time evolution of the mixing field is obtained with an error of  $< 1$  fs, i.e., small compared with the optical cycle of the 800 nm field. Figure 5 shows the spectrum of the XUV output versus delay time of the two beams. The time evolution for the different mixing fields can be analyzed in the wavelength range around 30 nm where the spectral resolution of the spectrometer is high. We measure the intensity of the mixing peak with high spectral resolution versus time delay of the 800 nm fields. These results are shown in the inset of Fig. 5 for some mixing field. For negative times delay the intensity of the mixing field increases rapidly and its profile is similar to that of the intensity of the laser pulses. For positive delay times the decay time is longer than the pulse duration and some oscillations of the mixing field intensity can be observed. The decay time reflects the coherence time of the free electron wave-packet. It is interesting to see that the time evolution of the mixing field intensities are related to the intensity envelope of the laser field and we cannot see the high frequency (optical cycle) oscillation.

## 5. COHERENT DIFFRACTIVE IMAGING WITH EXTREME ULTRAVIOLET SOURCE

In the coherent diffractive imaging technique a coherent light source is used to illuminate an object and the intensity of the diffraction pattern of the object is recorded. When a sample described by the complex transmission function  $T(r)$  is illuminated with a coherent, plane-wave light field, the diffracted image in the far-field is the Fourier transform of the sample. An inverse Fourier transform is applied to reconstruct the sample image from the intensity distribution of the diffraction pattern and the phase information. However, because only the diffraction amplitude can be captured, an iterative phase retrieval algorithm is used to recover the phase information [2,8]. Coherent diffraction imaging (CDI) in its original concept has a plane-wave geometry and requires a high degree of spatial coherence of the light source. The principle of CDI is simple, and a similar technique has been used in X-ray crystallography, but the experimental realization of CDI is much more difficult. In crystallography the weak signal diffracted from a unit cell of a large crystal is accumulated coherently and the periodic arrangement of the atoms acts like an amplifier so that detection of the Bragg peaks is straightforward. The diffraction pattern from a non-crystalline specimen or a nano-crystal has a much weaker intensity distribution which requires a very high flux source for illumination. The incident beam needs to be highly coherent and the coherence length is related to the over-sampling ratio of the diffraction pattern. For high resolution the diffraction intensity at high-angle diffraction needs to be recorded and in order to obtain high-quality diffraction patterns the dynamic range and quantum efficiency of the detector need to be high. Iterative retrieval of the phase of the far-field diffraction pattern permits reconstruction of the diffracting object with a spatial resolution that is limited, in principle, only by the wavelength of the incident radiation and the properties of the detector.

In order to increase the photon flux at the sample spot the harmonic beam is focused into the sample by a pair of mirrors comprising a plane mirror and a 20 cm-radius focusing mirror (commercial Optix Fab multilayer Mo/Si mirrors with 2 nm bandwidth and 35% reflectivity at 30 nm) which are installed in a Z-configuration to reduce astigmatism of the focusing. By using narrow bandwidth reflective and focusing mirrors, a single harmonic at around 30 nm (27th harmonic) is isolated and focused into the sample while the contributions of the two neighbouring harmonics is negligible, leading to a small bandwidth source ( $\lambda/\Delta\lambda > 250$ ). Consequently, the illumination field can be considered as a monochromatic source for the image reconstruction process. The degree of spatial coherence of the HHG source,  $\sim 0.99$ , which is obtained from the intensity distribution of the fringe contrast in a Young's double slit (YDS) experiment, indicates the very high spatial coherence of the HHG source [8].

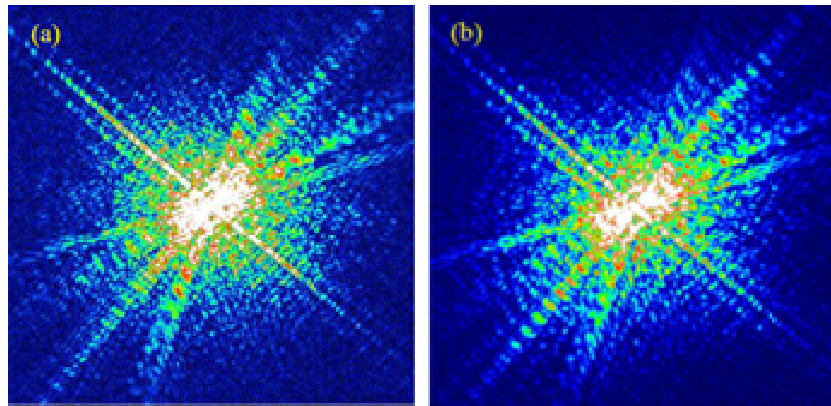


Figure 6: Diffraction images from a  $3\mu\text{m} \times 3\mu\text{m}$  sample at distances of (a) 1.5 mm and (b) 1 mm from the focus.

The test sample  $3\mu\text{m} \times 3\mu\text{m}$  is fabricated on a 50 nm thick  $\text{Si}_3\text{N}_4$  membrane and the sides are coated with 50 nm and 150 nm thick gold layers. The thinnest line in the test samples is 75 nm wide as shown in the scanning electron microscope images of the samples (Fig. 7a). The sample is mounted on a sample holder which allows precision alignment in the three directions  $x$ ,  $y$  and  $z$  using an  $x$ - $y$ - $z$  motorized translation stages. The diffracted emission of the sample after illumination with the focused harmonic beam is detected by a deep-cooled 16-bit resolution CCD camera (Princeton Instruments PIXIS 2048 x 2048) with  $13.5 \times 13.5\mu\text{m}$  pixel size. The camera is placed 3.5 cm behind the sample and is cooled to  $-40^\circ\text{C}$  to minimize thermal noise when taking diffraction data. At distances of  $\pm 1.5$  mm from the focus point the full width at half maximum (FWHM) of the source is  $> 15\mu\text{m}$ . Therefore, we expect the condition of uniform field over the sample is satisfied at positions of  $\pm 1.5$  mm from the focus. With an exposure time of 8 s (Fig. 6a)

a diffraction pattern with a high diffraction angle and a rather high signal-to-noise (S/N) image is obtained with the maximum dynamic range of our CCD. At distance  $\pm 1$  mm from the focus the FWHM of the beam is  $12 \mu\text{m}$  and the exposure time required to obtain the diffraction image is reduced to 4 s (Fig. 6b), but a new diffraction feature produced by a variation of the phase of the illuminating field is observed.

An image reconstruction is performed based on the Fraunhofer diffraction of a plane field by considering the phase variation of the illuminating field at the sample plane. The Error Reduction and Hybrid Input Output algorithm [12] is used to recover the sample's image. The plane-wave field code without considering the phase variation in the sample plane can be used for reconstruction of the sample from its diffraction image at the position  $-1.5$  mm after the focus. The recovered image is shown in Fig. 7b. Similar results are obtained for other positions, at  $+1.5$  mm from focus. This shows that the curvature of the beam has less influence on the diffraction image and the diffraction of a plane-wave field can be considered if the sample is not located close to the focus and the FWHM of the beam is much larger ( $>$  four times) than the total sample size.

The letter 'I' in the small sample and the gap within the letter which has a width of only  $75$  nm are clearly seen in the reconstructed image. The knife-edge test of the small image (shown in Fig. 7c) reveals that a resolution of  $\sim 45$  nm (10% to 90% of the intensity profile) is achieved, which matches the theoretical calculation ( $\delta=0.61 \lambda/\text{NA} = 46$  nm; the Rayleigh criterion) reasonably well. This resolution is limited by the pixel size and the size of the diffraction data that can be captured.

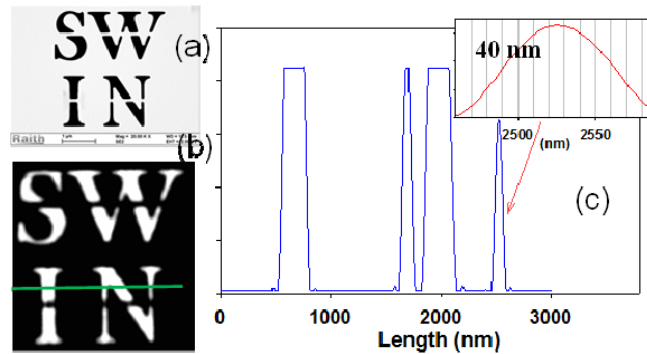


Figure 7: (a) Scanning electron microscope image of the test sample. (b) Reconstructed image of the sample at distances of  $1.5$  mm from the focus with a plane-wave field code. (c) Knife-edge test to determine the resolution of the reconstructed image of the small sample. The cross section is taken at the horizontal line in (b).

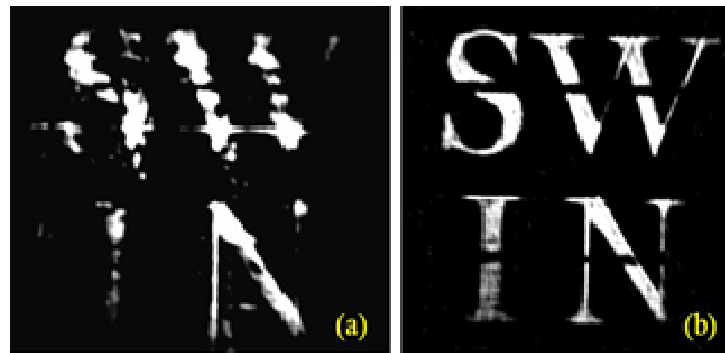


Figure 8: Reconstruction of the image of the sample at a small distance of  $1$  mm from the focus with a plane-wave field (a) and an additional phase variation (b).

When the sample is located close to the focus at  $-1$  mm the reconstructed image becomes blurred, despite a short exposure time. Figure 8a shows the reconstruction of a large sample from the diffraction image at  $-1$  mm when a plane-

wave field code is applied. The field intensity at the sample plane can still be considered to be homogeneous but the phase differs from that of a plane-wave field and the expected diffraction is distorted by the phase variation of the wave field at the sample plane. The reconstructed image is improved when the phase variation of the illuminating field is considered and we obtain an image (Fig. 8b). When the sample is at a distance  $< -1$  mm from the focus for a large sample it is not possible to use a plane-wave field code for reconstruction; however the sample can be reconstructed by considering the phase and intensity variation at the sample plane, especially for reconstruction of a small sample.

## 6. CONCLUSION

We have demonstrated the importance of phase matching in the HHG process. The phase matched generation can be used to control and enhance extreme ultraviolet radiation in terms of spectrum and intensity. The combination of two laser fields with controllable intensity opens a new way for the generation and amplification of extreme ultraviolet radiation which is a step towards obtaining attosecond pulses with high intensity. We confirm that a perturbative formalism can be developed around the generation and amplification process, up to ultra-high orders of nonlinearity. A perturbative treatment in the high-order harmonic frequency region will help in the investigation of quantum effects in atoms and molecules in the high photon energy range. We have also demonstrated that a high spatial resolution image ( $< 45$  nm resolution) can be reconstructed from a diffraction pattern generated by a table-top high-harmonic source at a wavelength of around 30 nm. This experiment is promising for imaging sub-10 nm objects, by using shorter wavelength radiation and a shorter distance from the object to the detector.

## REFERENCES

- [1] Smirnova, O., Mairesse, Y., Patchkovskii, S., Dudovich, N., Villeneuve, D., Corkum, P., Ivanov, M. Yu., “High harmonic interferometry of multi-electron dynamics in molecules”, *Nature* 460, 972 (2009); Worner, H. J., Bertrand, J. B., Kartashov, D. V., Corkum, P. B., and Villeneuve, D. M., “Following a chemical reaction using high-harmonic interferometry”, *Nature* 466, 604 (2010).
- [2] Chen, B., et.al. “Multiple wavelength diffractive imaging”. *Phys. Rev. A* 79, 023809 (2009).
- [3] Dao, L.V., Hall, C., Vu, H.L., Dinh, K.B., Balaur, E., Hannaford, P., Smith, T.A., “Phase-matched generation of highly coherent radiation in water window region”. *Appl. Opt.* 51, 4240 (2012).
- [4] Lewenstein, M., Balcou, P., Ivanov, M.Y., L’Huillier, A., Corkum, P. B., “Theory of high-harmonic generation by low-frequency laser fields”. *Phys. Rev. A* 49, 2117–2132 (1994).
- [5] Balcou, P., Salieres, P., L’Huillier, A., Lewenstein, M., “Generalized phase-matching conditions for high harmonics: The role of field-gradient forces”, *Phys. Rev. A* 55, 3204-3210, 1997.
- [6] Dao, L. V., Dinh, Kh. B., Hannaford, P., “Perturbative optical parametric amplification in the extreme ultraviolet”, *Nature Communi.* 6, 7175 (2015).
- [7] Dao, L. V., Dinh, K. B., and Hannaford, P., “High order harmonic generation for study of atomic and molecular dynamics”, *Appl. Phys. Lett.* 103, 141115 (2013).
- [8] Le, H. V., Dinh, K. B., Hannaford, P., Dao, L. V., “High resolution coherent diffractive imaging with a table-top extreme ultraviolet source”, *J. of Appl. Phys.* 116, 173104 (2014).
- [9] S. Teichmann, B. Chen, R.A. Dilanian, P. Hannaford, L. V. Dao, “Spectral characteristics across the spatial profile of a high-harmonic beam”, *J. Phys. D: Appl. Phys.* 42, 135108 (2009) ; Teichmann, S., Hannaford, P., Dao, L.V., “Phase-matched emission of few high-harmonic orders from a helium gas cell” *App. Phys. Lett.* 94, 171111 (2009).
- [10] Worner, H.J., Niikura, H., Bertrand, J. B., Corkum, P. B., Villeneuve, D. M., “Observation of Electronic Structure Minima in High-Harmonic Generation”. *Phys. Rev. Lett.* 102, 103901(4) (2009).
- [11] Bertrand, J. B., et al. “Ultrahigh-order wave mixing in noncollinear high harmonic generation”. *Phys. Rev. Lett.* 106, 023001(4) (2011).